Materials Research. 2014; 17(3): 570-582
DOI: http://dx.doi.org/10.1590/S1516-14392014005000054

Comparative Study of the Characteristics of Nano Silica–, Silica Fume– and Fly Ash–Incorporated Cement Mortars

Hasan Biricik*[a], *Nihal Sarier*[b]

[a]*Department of Civil Engineering, Maltepe University, Marmara Campus, 34857, Maltepe, Istanbul, Turkey*
[b]*Department of Civil Engineering, Istanbul Kültür University, Atakoy Campus, 34156, Bakirkoy, Istanbul, Turkey*

Received: June 3, 2013; Revised: December 9, 2013

The structural characteristics of cement mortars, impregnated with nano silica (NS), silica fume (SF) and fly ash (FA), were comparatively studied using Fourier transform infrared spectrometer (FTIR), thermogravimeter-differential thermogravimeter (TG-DTG) and scanning electron microscope (SEM). The mechanical strengths of the specimens were determined at early (7th day) and standard (28th day) curing ages. The compressive strengths and flexural strengths developed in the mortar specimens containing NS particles were found considerably higher than those of the corresponding specimens of SF and FA over and above the control at both ages. FTIR, TG-DTG and SEM analyses results were consistent with the remarkable increase in the mechanical strength of the mortars with NS. These increases in the strengths of the mortars with NS are attributable to the nano sized particles and extensive surface area of NS. The nano sized particles, as nucleating agents, promoted the hydration of C_3S and C_2S and the formation of C–S–H phase. Plenty of active sites on the surface of NS particles induced their pozzolanic reactivity and the extent of bond formation between NS particles and free CH.

Keywords: *nano silica, silica fume, fly ash, mortar, FTIR, TG–DTG*

1. Introduction

The cement industry is considered to be one of the most energy consuming industries, which is also responsible for approximately 6-7% of the global man-made CO_2 emissions annually[1-4]. Accordingly, there is a great demand to minimize the quantity of cement used in the construction industry[4]. In this context, supplementary cementing materials (SCMs) with pozzolanic or hydraulic properties have been particularly attractive compounds or mixtures which partially replace ordinary Portland cement required for a cement-based composite[5,6]. The most widely used SCMs in cement composites are fly ash (FA) and silica fume (SF), that are obtained as the by-products of the coal industry and the silicon-ferrosilicon industries, respectively[7,8]. FA and SF enhance mainly the long-term strength and durability properties of cement composites owing to their pozzolanic reactions with calcium hydroxide formed during the hydration of calcium silicates[7-11]. However, there are some concerns about cement composites incorporated with FA or SF. For example, the strength development of FA concrete, particularly that containing Class F fly ash, is slow compared to normal concrete that is not suitable for many applications where early strength is required, such as repairs and rapid construction[5,6]. Whereas, concretes containing SF are thought to be more susceptible to plastic shrinkage than any other type of concrete, particularly in structures with large surface areas[12].

Recently, impregnation of nanoparticles into ordinary Portland cement (OPC) paste, mortar and concrete has received particular attention as a promising research field for nanocomposites, which can produce superior mechanical and physical properties in OPC composites. This nanocomposite technology can be applied directly to the construction industry[13]. Previous research indicates that the inclusion of nanoparticles improves fresh and hardened state properties, even when compared with conventional mineral additions[13-15]. Among these nanoparticles, nano SiO_2 (nano silica, NS) is becoming an increasingly important component of special concretes and other advanced cement based materials[8,15-26]. It consists of amorphous silicon dioxide with a particle size at nano scale, having a high surface area to volume ratio, therefore providing the potential for tremendous chemical reactivity[1,2,14]. Currently, the prices of various NS products in the markets are higher than FA and SF which limit their commercial applications[27]. However, some latest studies have focused on developing new processes for reducing the raw material, energy consumption and cost in NS production[27,28].

Many research groups have conducted experiments on the microstructure, mechanical and physical properties of cement paste, mortar and concrete impregnated with NS[1,15-17]. These experimental studies have shown that NS causes great enhancement in compressive and flexural strengths, durability, modulus of elasticity, pore structure and resistance to ion penetration, and setting time of cement based materials[8,15-26]. When NS particles are included into hydrating OPC, they increase calcium silicate hydrate (C–S–H) gel formation as a result of the reaction of NS with $Ca(OH)_2$ (calcium hydroxide, CH), accelerate the

*e-mail: n.sarier@iku.edu.tr

hydration of tricalcium silicate (C_3S) and dicalcium silicate (C_2S) and fill spaces in the C–S–H crystal lattice, acting as a nano-filler[16,21,29]. Furthermore, NS decreases the setting time of mortar and reduces bleeding water and segregation while improving the cohesiveness of mixtures in the fresh state[29]. On contrary, there are two important problems to be considered regarding use of NS in cement composites. One important difficulty is dispersing NS particles in a cement mixture. The previous studies showed that the dispersion method of the NS particles affects the workability of cement mortar, the rate and extent of cement hydration as well as the structural, physical and mechanical properties of the fresh and hardened cement composites[11,30-33]. Some authors have concluded that the appropriate percentage of NS must be small (1-5 wt%) to avoid agglomeration of particles during mixing[12-16], while others have indicated that properties can also be improved with higher dosages up to approximately 10 wt% if these nanoparticles are successfully dispersed in the initial cementious mixture[7,12,17,29]. Second problem related with using NS in a cement mixture is the decrease in fluidity, due to its high surface area and increased water demand[29-34]. Some research groups have studied the interaction of superplasticizers with NS added cements, and reported that the type and concentration of superplasticizer, along with the particle size and surface area of NS, affect the rheological properties of fresh cement mixtures[29-34]. Very recently, the effects of morphological and textural characteristics of different amorphous nano silica's on mechanical properties of standard mortars were studied, and the main parameters influencing the mechanical properties of cement mortars were reported as the specific surface area, the micropore volume and the average size of the primary particles of the silicas[28,35]. In the view of all these intensive studies, it sounds that developing and characterization of new NS based cement composites with improved mechanical performance and durability continue to draw attention as an open-ended research topic for promoting the appropriate use of nano silica at the industrial scale in construction sector.

In the present study, the achievability of using 5 wt% and 10 wt% of NS to reduce cement consumption in mix proportions of cement mortars while improving their mechanical strength was investigated. The influence of the high dosages of NS on the compressive and flexural strengths and structural properties of cement mortars at early (7th day) and standard (28th day) curing ages were compared with the effect of equal amounts of SF and FA. The structural changes of mortar specimens were characterized by Fourier transform infrared spectrometer (FTIR), thermogravimeter-differential thermogravimeter (TG-DTG) and scanning electron microscope (SEM).

2. Experimental

2.1. *Materials*

Nano SiO_2 (Silicon dioxide 4850MR® or NS) in powder form was purchased from NanoAmor, Inc. (Houston, TX). A specific gravity of 2.2-2.4 at 25 °C, bulk density of 0.068 $g.mL^{-1}$, average particle size of 15 nm and specific surface area of 640 $m^2.g^{-1}$ were the listed physical properties of this batch of NS[36]. The silica fume (SF) and the F type fly ash (FA) were from Eti Krom Inc. (Istanbul, TR) and Yatagan Thermal Plant (Yatagan, TR), respectively. The particle size distributions of SF and FA were measured with a Malvern Nanosizer ZS3600 at λ=633 nm, using 0.01% dilute SF and FA suspensions in isopropyl alcohol at 25 °C. Multipoint BET surface area measurements of SF and FA were conducted using a Quantachrome Nova4000E at 77.3 K with nitrogen as the adsorbent gas. The particle size, specific surface area and specific gravity values of NS, SF and FA are listed in Table 1. The SEM images of NS, SF and FA used in this study are shown in Figure 1.

Table 1. The chemical compositions of OPC, NS, SF and FA as reported by the suppliers and their specific gravity, mean particle size and specific surface area (BET) values.

Constituents	Content (wt%)			
	OPC	NS	SF	FA
SiO_2	20.6	99.5	83.9	56.3
Al_2O_3	4.5	<0.004	0.5	32.1
Fe_2O_3	3.2	<0.001	1.3	3.9
Na_2O	0.3	–	0.5	0.1
K_2O	0.8	–	2.9	-
CaO	64.0	<0.003	1.4	3.9
MgO	1.2	<0.002	4.8	1.4
Cr_2O_3	0.3	–	0.6	–
SO_3	3.1	–	1.3	–
Loss on ignition at 1000 °C	1.4		2.5	2.2
	Physical properties			
Property	OPC	NS*	SF	FA
Specific gravity (at 25 °C)	3.14	2.20-2.40	2.21	2.20
Mean particle size (nm)	15.5×10^3	15.0	444.2	1513.0
BET surface area ($m^2.g^{-1}$) (±0.05)	3.99×10^{-1}	640.00	13.90	2.60

*Listed properties provided by the supplier's data sheet[36]

Ordinary Portland cement (OPC) with a specific gravity of 3.14 and classified using the TS EN 197-1 standard was obtained from Akcansa Cement Inc. (Istanbul, TR). Commercial silica sand with a maximum particle size of 2.0 mm, specific gravity of 2.63 and fineness modulus of 2.91, was purchased from Pınarhisar Cement Inc. (Kırklareli, TR) and used as an aggregate in the mortar. The superplasticizer admixture, prepared as defined in the CSN EN 934-2 standard[37], was polycarboxylic acid based (Sika® ViscoCrete® Hi-Tech 32) with a density between 1070 and 1110 kg.m^{-3}, an alkali content of less than 4% of Na_2O, and a chloride ion content of less than 0.1%. The chemical compositions of OPC, NS, SF and FA reported by the suppliers are given in Table 1.

2.2. *Preparation and characterization of the cement mortar specimens*

To obtain colloidal dispersions of NS, SF or FA, a known amount of the additive was mixed with 225 g of distilled water and stirring was performed at 15,000 rpm with IKA T 25 digital Ultra-Turrax® Homogenizer for 2 min at room temperature. Consequently, the physical attractions between NS, SF or FA particles were overcome and new physical attractions, especially hydrogen bonding between O atoms of SiO_2 and OH groups of water molecules were obtained, which triggered the pozzolanic reactivity of the particles[8,16,20]. For each sample, a known amount of polycarboxylic acid based superplasticizer was added into the colloidal dispersion over 30 s at 120 rpm to prevent flocculation and water entrapment in the flocks, reducing the amount of water needed to obtain comparable fluidity[32,33]. The mixture was left to rest for 1.5 min and then stirred further at 120 rpm for 1 min. Next, a known amount of cement and 350 g of sand were added to the dispersion while stirring at 120 rpm for 1 min. Each mixture was instantly poured into a stainless steel mold (40 mm × 40 mm × 160 mm) on a vibrator plate enabling compaction. One day later, the demolded mortar specimens were cured in a lime-saturated water bath at 20±2 °C until they were tested. The cement mortars were prepared with water to cement ratio of 0.5. In order to achieve a constant workability, the appropriate amounts of water and superplasticizer to be added into a mortar mixture, were predetermined by measuring the mean diameter (R´) of a test sample on flow table according to CEN EN 1015-3 standard[38]. The flow tests were repeated, using a fresh batch of mortar each time, until the desired flow was achieved. Table 2 illustrates the mixture proportions, spread ratios and bulk densities of the mortar specimens.

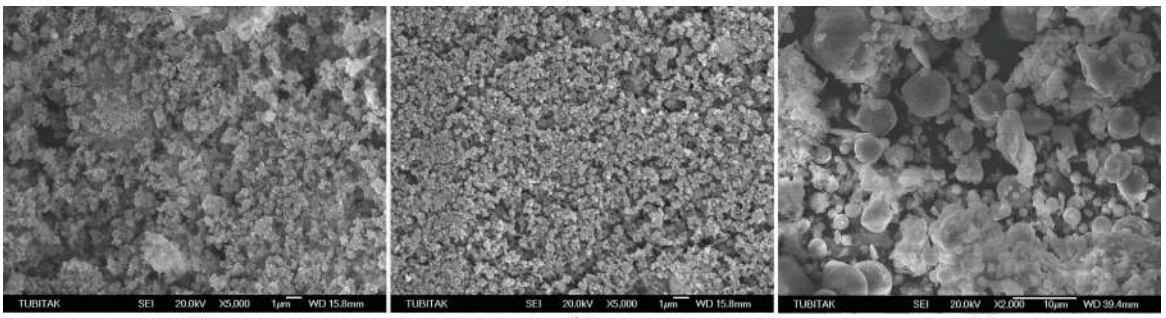

Figure 1. SEM images taken in this study for the pozzolanic additives: a) NS, magnification x5,000; b) SF, magnification x5,000; and c) FA, magnification x2,000.

Table 2. Mixture proportions, spread ratios and bulk densities of the mortar specimens (water to cement ratio =0.50).

Sample	Type and amount of mineral additive	Amount of superplasticizer (g)	Amount of cement (g)	Spread ratio (R´/100)	Bulk density (kg.dm^{-3})
OPC	-	0.0	450.0	1.00	2.16
NS5	22.5 g NS (5 wt%)	5.0	427.5	1.03	2.13
NS10	45.0 g NS (10 wt%)	10.0	405.0	1.00	2.12
SF5	22.5 g SF (5 wt%)	1.0	427.5	1.00	2.14
SF10	45.0 g SF (10 wt%)	2.0	405.0	1.00	2.13
FA5	22.5 g FA (5 wt%)	1.0	427.5	1.00	2.15
FA10	45.0 g FA (10 wt%)	2.0	405.0	1.00	2.14

Compressive and flexural strength experiments of the specimens were performed at early and standard curing ages according to ASTM C39/C39M–12 and ASTM C348–08 Standards[39,40], respectively, using a FORE FR–BC293–type united testing system equipped with 20 kN and 200 kN load cells, respectively, and attached to a computer interface for data acquisition. The loading speed was 0.24 MPa.s^{-1}.

Changes in the structure of the mortar specimens, including those with 10 wt% NS, SF or FA, were examined with a Perkin Elmer Spectrum 100 Fourier transform infrared spectrometer (FTIR) equipped with a universal attenuated total reflection (ATR) accessory. Thermogravimetric and differential thermogravimetric (TG-DTG) analyses of the samples were performed from 20 to 1000 °C at 10 °C.min^{-1} rate under a dry nitrogen atmosphere purged with a SEIKO 6200 TG/DTA instrument at 20 mL.min^{-1} rate. The TG/DTA instrument was calibrated with indium, and platinum pans were used as sample holders. For TG-DTG analysis, a sample was taken from the center of each specimen, then grinded into a powder. The approximate sample mass was 100 mg per sample. TG-DTG experiments were repeated for three different samples of each specimen. Scanning electron microscopy (SEM) analyses were performed using a JEOL JXA840A type SEM instrument. For preparation of the SEM samples, approximately 0.01 g of a sample taken from the middle of each mortar specimen was placed on standard mounts 15 mm in diameter and 2 mm in depth under a vacuum and coated with a 1-2 nm thick conductive layer of gold to prevent charging prior to imaging. The applied voltage and current values were 40.0 kV and 30.0 mA, respectively.

3. Results and Discussion

3.1. *Mechanical strength results*

Compressive and flexural strength data for all of the specimens as a function of the extent of hydration are presented in Figure 2 and 3, respectively. As given in Figure 2a, the compressive strength of OPC was 28.7 MPa after 7 days of curing. At early age, the compressive strength of the NS5, SF5 and FA5 specimens with 5 wt% mineral additives was 31.4 MPa, 28.5 MPa and 22.7 MPa, respectively. The compressive strength of NS5 was 9.5% greater than that of OPC. Conversely, 5 wt% mineral addition in SF5 and FA5 did not result in improvement in the compressive strength in comparison to OPC after 7 days of curing. That is to say, the compressive strength of SF5 was very close to that of OPC while the compressive strength of FA5 was lower than that of OPC at early age. After 28 days of curing, the compressive strength of OPC was measured as 31.9 MPa. At this standard age, the compressive strength of the NS5 and SF5 specimens ascended to 41.9 MPa and 39.6 MPa, and the corresponding increases in their

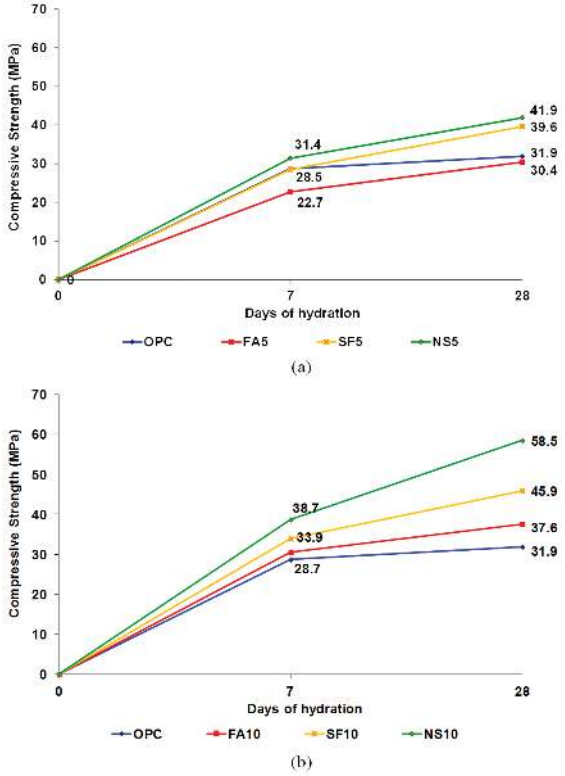

Figure 2. Compressive strength of the mortar specimens versus days of hydration: a) the specimens with 5 wt% mineral additive and the control; b) the specimens with 10 wt% mineral additive and the control.

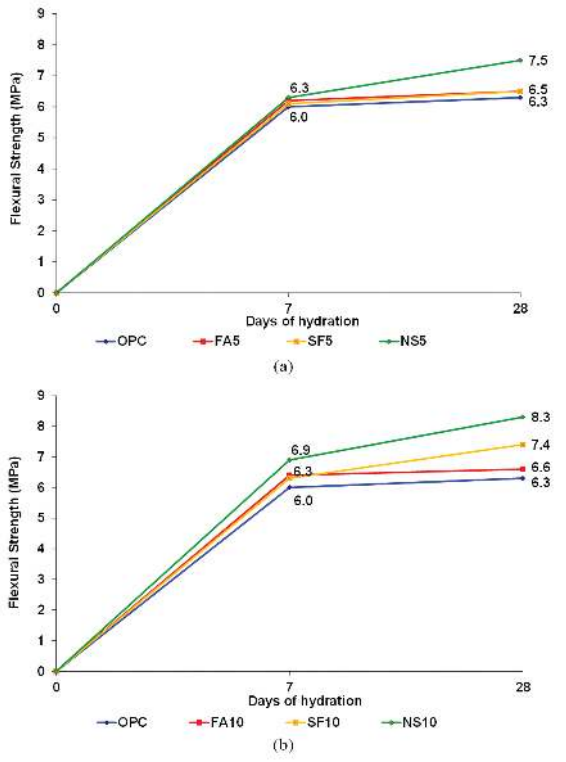

Figure 3. Flexural strength of the mortar specimens versus days of hydration: a) the specimens with 5 wt% mineral additive and the control; b) the specimens with 10 wt% mineral additive and the control.

compressive strength, compared to OPC, were calculated to be 32% and 24%, respectively. On the contrary, the compressive strength of FA5 was measured 30.4 MPa at the age of 28 days, which was slightly lower than that of OPC.

As seen in Figure 2b, when the amount of mineral additive was increased to 10 wt%, in the NS10, SF10 and FA10 specimens, compressive strengths reached 38.7 MPa, 33.9 MPa and 30.6 MPa, respectively, at 7 days. These increases in the compressive strength of NS10, SF10 and FA10, compared to OPC, were calculated as 35%, 18% and 7% respectively. After 28 days of curing, the compressive strength of NS10, SF10 and FA10 increased to 58.5 MPa, 45.9 MPa and 37.6 MPa, respectively. The corresponding increases in the compressive strength of NS10, SF10 and FA10, compared to that of OPC, were calculated as 84%, 44% and 18%, respectively.

As seen in Figure 3a, the flexural strengths of the specimens with 5 wt% mineral additive (NS5, SF5 and FA5) were in the range of 6.1 MPa–6.3 MPa, which were slightly higher than that of OPC (6.0 MPa) at early age. After 28 days of curing, the flexural strength of the mortar specimen NS5, with 5 wt% NS, ascended to 7.5 MPa, while the flexural strengths of the SF5 and FA5 specimens were approximately 6.5 MPa, on par with OPC (6.3 MPa) (see Figure 3a). The flexural strength of NS5 was 19% higher than that of OPC at standard age.

The flexural strengths of the specimens with 10 wt% mineral additive (NS10, SF10 and FA10), given in Figure 3b, were in the range of 6.3 MPa–6.9 MPa, which were slightly higher than that of OPC (6.0 MPa) after 7 days of curing. On the other hand, after 28 days, the flexural strength of NS10, with 10 wt% NS, increased to 8.3 MPa, while the flexural strengths of SF10 and FA10 with 10 wt% SF and FA additives were measured as 7.5 MPa and 6.5 MPa, respectively. The flexural strength of NS10 was the highest across all the specimens and 32% higher than that of OPC at standard age.

3.2. *Characterization of the mortar specimens*

FTIR transmission spectra of the mortar specimens, including 10 wt% of NS, SF and FA after 7 days and 28 days of curing, are presented in Figure 4.

The broad bands appearing at 3648-3650 cm^{-1} in the spectra of all mortar specimens including OPC (control) corresponded to the overlapping stretching vibrations of the structural –OH groups (ν_3) of $Ca(OH)_2$ formed during the hydration of C_3S and C_2S, and the free –OH groups (ν_1) of water molecules present in the mixture[41,42]. This band diminished for all samples as the hydration process proceeded, implying a decrease in free water due to C–S–H bond formation[43]. The decrease in the intensity of this band for NS10 and SF10 were the most pronounced after 28 days of hydration. Furthermore, the 3650 cm^{-1} band of NS10 had nearly disappeared, suggesting increased consumption of C_3S and C2S phases and also increased formation of C–S–H phase compared to SF and FA, over and above the pozzolanic reactivity of NS for $Ca(OH)_2$[1].

The broad band observed at 3411 cm^{-1} in the IR spectra of OPC corresponded to overlapping stretching vibrations of both the structural and free –OH groups of CH, C–S–H and water, respectively[1,41]. The intensity of the 3411 cm^{-1} band of OPC did not change after 28 days of curing, while that of FA10 decreased a little. This band shifted slightly to 3410-3390 cm^{-1} and became broader and smaller in the IR spectra of the NS10 and SF10 specimens. This phenomenon indicated a decrease in the amount of bonded –OH groups and free water, signifying reduction in $Ca(OH)_2$ content, and increase in C–S–H content in NS10 and SF10[1,41-44]. The bending-in-plane vibrations of the –OH groups (ν_2) of free water molecules are characterized by a small broad band

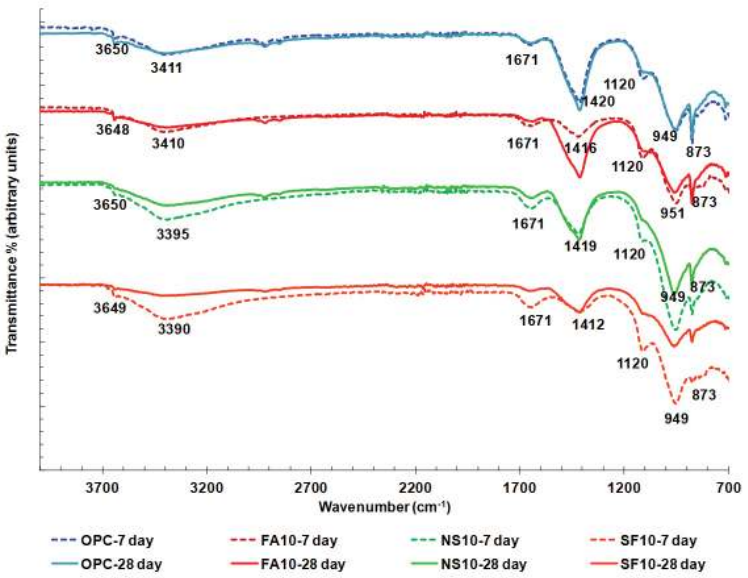

Figure 4. FTIR transmission spectra of the mortar specimens containing 10 wt% of NS, SF and FA after 7 days (… dashed line) and 28 days (– solid line) of curing.

at 1671 cm^{-1}. Similar to the stretching vibrations, this band had lower intensities in the spectra of the NS10 and SF10 specimens compared to the OPC and FA10 samples after 28 days, confirming the decrease in free water due to C–S–H formation, which occurred faster than in OPC and in FA10[1].

The FTIR spectrum of OPC showed two distinct peaks at 1420 cm^{-1} and 873 cm^{-1}, corresponding to the stretching and bending-in-plane vibrations of the C–O bonds of CH and $CaCO_3$, resulting from the reaction between $Ca(OH)_2$ and CO_2 in the air[45-47]. The intensity of the 1420 cm^{-1} band is assumed to be closely related with the ratio and depth of carbonation[46,47]. The 1420 cm^{-1} band shifted slightly to 1412-1419 cm^{-1} in the FTIR spectra of the NS10, SF10 and FA10 specimens after 7 days and 28 days of curing. The intensities of the 1412-1419 cm^{-1} band of NS10 and SF10 were smaller than that of FA10 and the control at standard age suggesting the decrease in carbonation ratio and depth in these samples[45-47]. Similar to the stretching vibrations, the bending-in-plane vibrations of the C–O bonds at 873 cm^{-1} had lower intensities in the IR spectra of the NS10 and SF10 specimens at standard age[46].

The band appeared at 1120 cm^{-1} in the FTIR spectrum of OPC, corresponding to the stretching vibrations of the S–O bond of gypsum and ettringite[44,47]. This band decreased in size as the curing time was extended in the spectra of FA10, SF10 and specifically in the FTIR spectrum of NS10 after 28 days reminding lesser extent of ettringite formation in NS10[44,46,47]. The strong band observed at 949 cm^{-1} and the band observed at 719 cm^{-1} were associated with the bending-in-plane vibrations of the Si–O bonds in tricalcium silicates (C_3S) and dicalcium silicates (C_2S)[1,40,42,47]. The intensity of these bending–in–plane vibrations of the Si–O

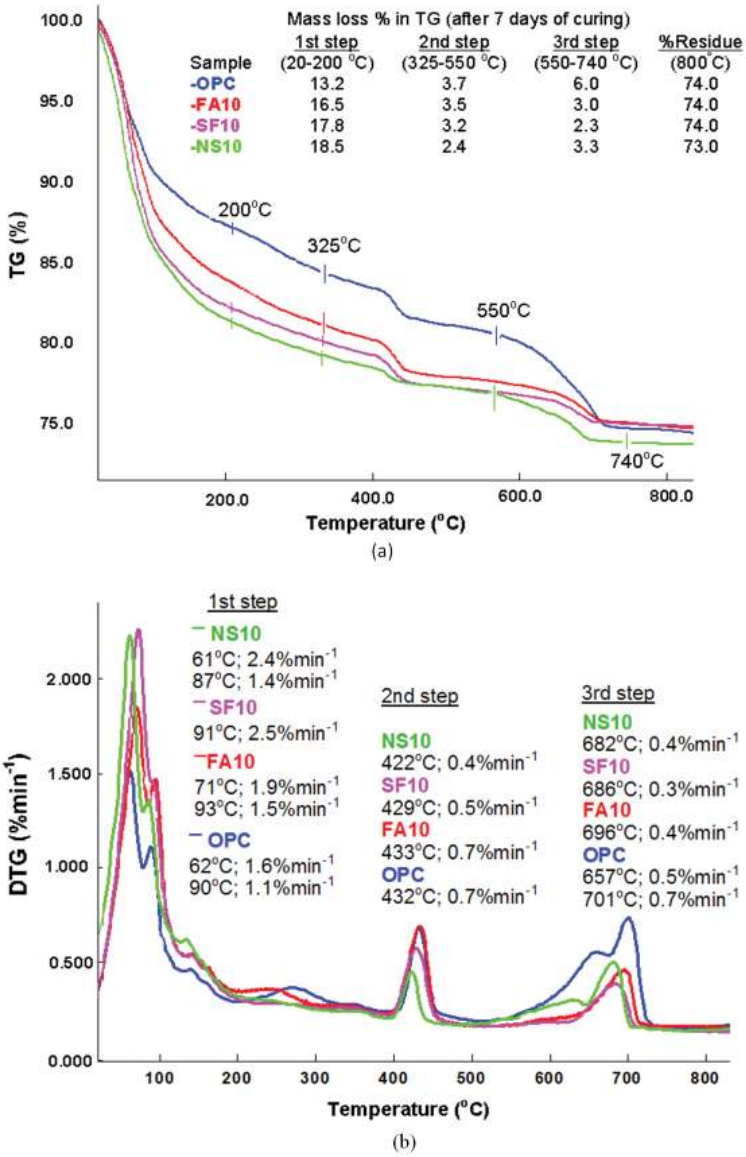

Figure 5. At the age of 7 days: a) TG and b) DTG curves of the mortar specimens containing 10 wt% of NS, SF and FA.

bonds decreased as C–S–H crystals formed[48]. The intensities of the 949 cm^{-1} band of OPC after 7 days of curing and 28 days of curing overlapped, indicating deceleration of C–S–H formation as the curing time was prolonged in OPC. Addition of NS, SF or FA into the cement mortar influenced the positions and intensities of these Si–O bending vibrations. The 949 cm^{-1} band shifted to 969-972 cm^{-1} and the 719 cm^{-1} band shifted to 730 cm^{-1} in the FTIR spectra of NS10, SF10 and FA10 after 7 days and 28 days, which have been defined as a fingerprint evidence for the degree of polymerization with the formation of C–S–H phase due to hydration[1]. The intensities of the Si–O bending bands of NS10 and SF10 after 28 days of curing dropped noticeably, while those of OPC and FA10 did not change significantly. These findings were further evidences for the polymerization of the silica groups and formation of C–S–H bonds in NS10 and SF10 as curing time was extended to 28 days[48]. After 28 days of curing, the lowest intensities were observed for the Si–O bending bands of the NS10 specimen, highlighting the highest degree of polymerization silica (SiO_4) units with the formation of C–S–H phase in NS10 compared to OPC, FA10 and even to SF10[19,48].

Figure 5a, 5b and Figure 6a, 6b present TG and DTG curves of the mortar specimens containing 10 wt% of NS, SF and FA after 7 days and 28 days of curing, respectively. TG-DTG curves show the typical reactions occurring in the cement mortars when subjected to a progressive temperature increase from room temperature to 1000 °C. The mass loss in the mortar specimens, including the control, during heating in the TG-DTG analyses occurred in three main steps. The dehydration of water molecules in hydrates such as C–S–H and ettringite took place within the range from room temperature to 200 °C[29,49-55]. The second step of thermal degradation occurred between 325-550 °C, and the corresponding mass loss was associated with the dehydroxylation of free CH produced during curing[29,49-55]. When the mortar specimens were cured, calcium hydroxide forming in them gradually combined with carbon dioxide of the surrounding air to form calcium carbonate[46]. The third decomposition step happened between 550-740 °C was due

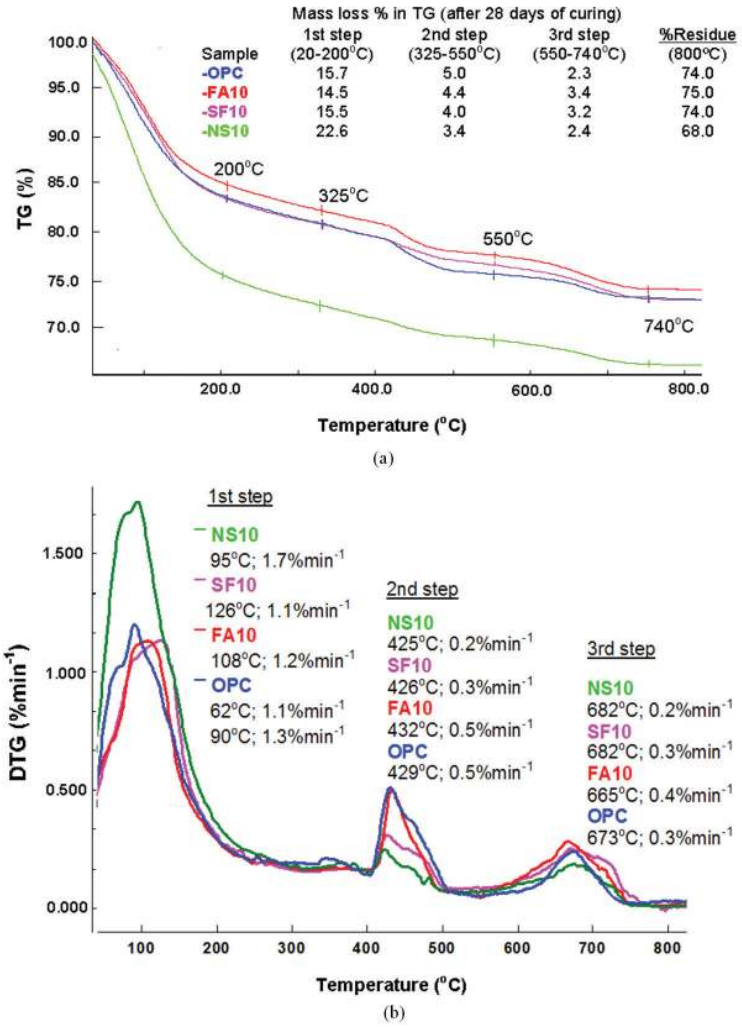

Figure 6. At the age of 28 days: a) TG and b) DTG curves of the mortar specimens containing 10 wt% of NS, SF and FA.

to decomposition of calcium carbonate and escape of CO_2 from the cement matrix[46,49-57]. Table 3 presents the mass percent of free CH, and the mass percent of $CaCO_3$ which were calculated by multiplying the mass loss percent of the second and third steps of TG curves, given in Figure 5a and 5b, with the stoichiometric molar mass ratios of $Ca(OH)_2$/H_2O and $CaCO_3/CO_2$, respectively, as mentioned in the literature[46,56,57].

At the age of 7 days, the TG curves of FA10, SF10 and NS10 showed similar changes to that of OPC, with some changes in mass loss and mass loss rates at each step. The first DTG peaks of OPC after 7 days of curing appeared at 62 °C and 89 °C, corresponding to a 13% mass loss on the TG curve up to 200 °C. Similarly, the first DTG peaks of FA10, SF10 and NS10 appeared between 61 °C and 93 °C in which the highest mass loss rates were observed for NS10

Table 3. Mass % of $Ca(OH)_2$ and of $CaCO_3$ calculated from the second and third steps of TG analyses for the mortar specimens containing 10 wt% of NS, SF and FA at the age of 7 days and 28 days.

Sample	Second step of TG		Third step of TG		Sum of second and third steps of TG	
	Mass% of $Ca(OH)_2$		Mass% of $CaCO_3$		Total mass% of $Ca(OH)_2$ and $CaCO_3$	
	7 days	28 days	7 days	28 days	7 days	28 days
OPC	15.2	20.6	13.6	5.2	28.8	25.8
FA10	14.4	18.1	6.8	7.7	21.2	25.8
SF10	13.2	16.4	5.2	7.3	18.4	23.7
NS10	9.9	14.0	7.5	5.4	17.4	19.4

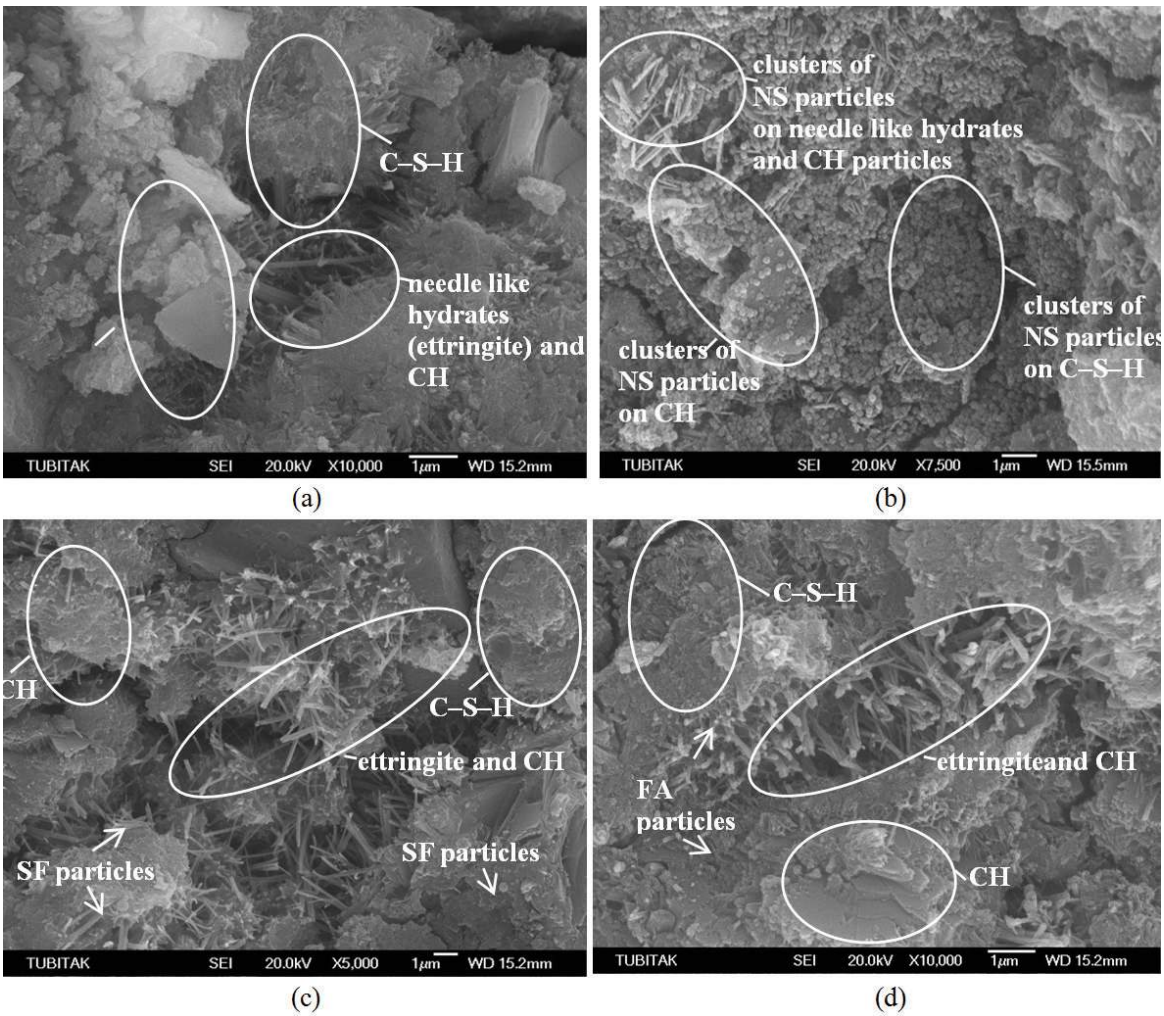

Figure 7. SEM images of the mortar specimens after 7 days of curing: a) OPC (control), magnification x10,000; b) NS10, magnification x7,500; c) SF10, magnification x5,000; d) FA10, magnification x10,000.

and SF10. The mass loss on the TG curves of FA10, SF10 and NS10 occurred in the first step were 16.5%, 17.8% and 18.5% respectively. This finding indicated the gradual increase in hydrated mineral phases for FA10, SF10 and NS10, where the highest percent of hydrated minerals was found in NS10. The second step of decomposition of OPC occurred between 325 °C and 550 °C, reached a maximum rate at 432 °C, resulting in a 3.7% mass loss. The second step of thermal decomposition of FA10, SF10 and NS10 occurred in the same temperature range, where the corresponding mass losses were 3.5%, 3.2% and 2.4% respectively. The third decomposition step of OPC, as well as those of FA10, SF10 and NS10, occurred between 550 °C and 740 °C. The mass loss rates observed at the third step of DTG showed a significant decrease in the rate of decomposition of calcium carbonate in FA10, SF10 and NS10 in comparison to that of OPC. The residues of FA10, SF10 and NS10 at 800 °C, as well as the control were about 73-74% at early age.

Figure 6a and 6b show the TG–DTG behavior of all the specimens after 28 days of curing. The significant points of the TG–DTG analysis at the age of 28 days can be summarized as follows: the incline of the first step of the TG curve of NS10 was very steep, the corresponding mass loss rate was the maximum (1.7 %.min^{-1}) and reached 22.6% mass loss at 200 °C, much greater than SF10, FA10 and OPC due to the higher extent of C–S–H formation in NS10[29,37,38]. The mass losses at the second step of TG analyses for FA10, SF10 and NS10, related to the decomposition of CH, were 4.4%, 4.0% and 3.4% respectively, which were all lower than 5.0% mass loss of OPC. The second thermal decomposition step of NS10 and of SF10 occurred considerably slower than those of OPC and FA10 as given in their DTG curves (Figure 6b). In the third decomposition step between 550 °C and 740 °C, the mass loss rate of NS10 observed was the smallest among all the samples. Residues of OPC, FA10 and SF10 at 800 °C were 74%, 75%, 74%, respectively, while the residue of NS10 was 68%.

Mass percent of $Ca(OH)_2$ and of $CaCO_3$ calculated from the second and the third steps of TG analyses for the mortar specimens containing 10 wt% of NS, SF and FA at the age of

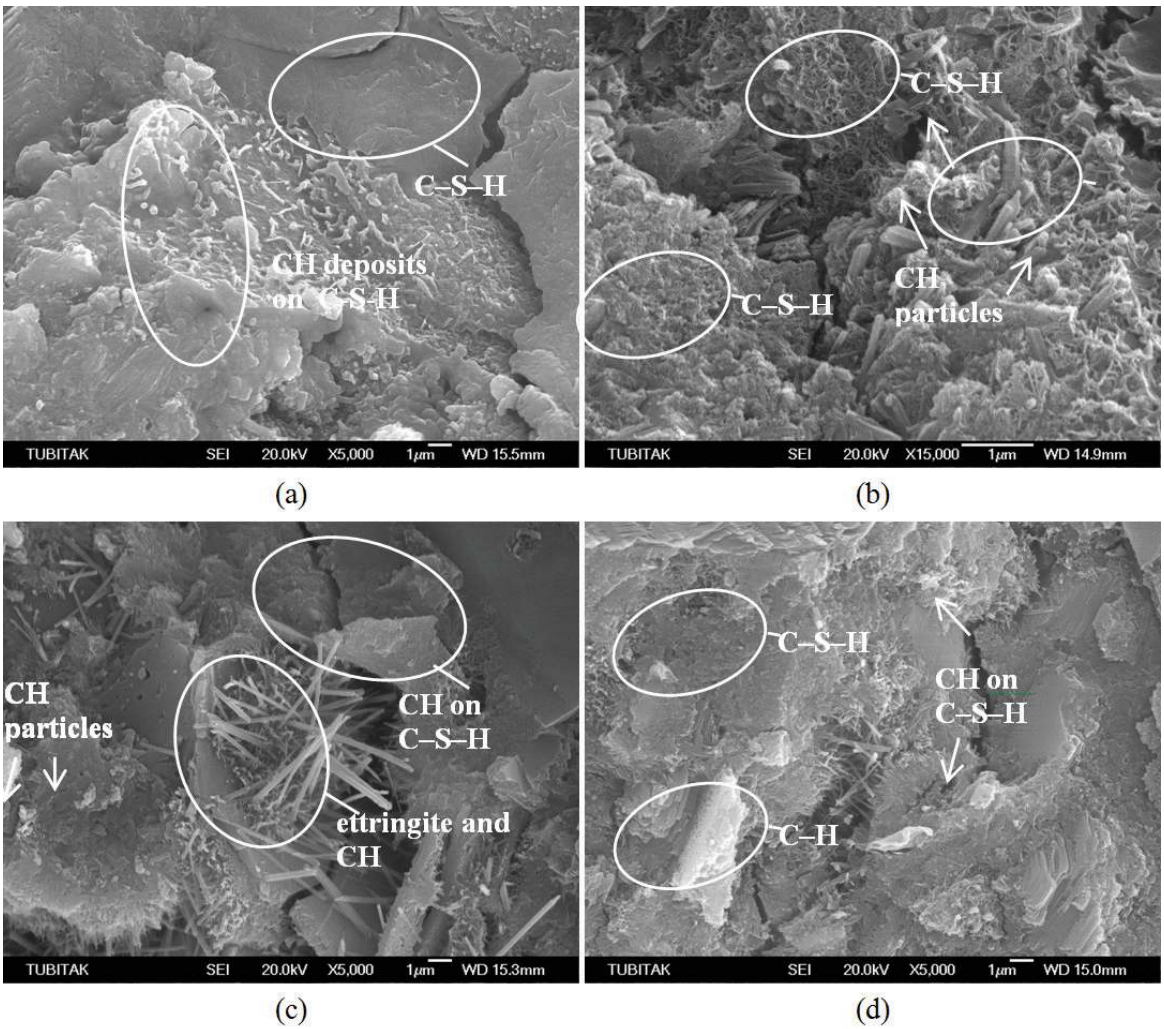

Figure 8. SEM images of the mortar specimens after 28 days of curing: a) OPC (control group), magnification x5,000; b) NS10, magnification x15,000; c) SF10, magnification x5,000; d) FA10, magnification x5,000.

7 days and of 28 days are given in Table 3. As seen in Table 3, at the age of 7 days, the mass percent of free CH, which did not enter the pozzolanic reaction, in FA10 and SF10 were calculated as 14.4% and 13.2%, both were very close to that of OPC (15.2%). Alternatively, the amount of free CH of NS10 was found the least among all the samples, i.e. 9.9%. In addition, the total amount of CH and calcium carbonate of NS10 was 17.4%, which was also the smallest among all the samples. These findings indicated the noticeable increase in the extent of bond formation between NS and free calcium hydroxide compared to bond formation of SF or FA with free CH at early age. At standard age, the amount of free CH and the total amount of CH and calcium carbonate for NS10 were calculated as 14.4% and 19.4% respectively. Both were considerably less than those of FA10 and SF10, indicating the rising extent of bonding between NS and free CH in NS10 in comparison to bonding in FA10 and SF10, and also suggesting the difficulty of CO_2 penetration in NS10 due to the strength of bond formation and compact structure of NS10. These results are in good agreement with FTIR results along with the higher compressive and flexural strengths observed in NS10.

SEM analyses were used to study the influence of NS, SF and FA on the microstructure of the OPC mortar. The SEM images of the fracture surfaces of OPC, NS10, SF10 and FA10 after 7 days of curing are shown in Figure 7. The fracture surface of the OPC sample is typical for a cement mortar, displaying a heterogeneous distribution of C–S–H and CH grains and needle–like ettringite crystals. Some micro cracks are visible within the structure. The SEM images of SF10 and FA10 after 7 days of curing are similar and show condensed packing of cement hydration products. The mineral particles SF or FA are arbitrarily dispersed throughout the hydrated cement products. The SEM images show CH and ettringite crystals between the C–S–H crystals[1,16,29,49,53,58]. The SEM image of the fracture surface of NS10 after 7 days illustrates a very condensed mortar structure and a good dispersion of NS clusters throughout the entire surface of hydrated cement products. The CH grains of NS10 are less visible than those of OPC, SF10 and FA10[49,52,59-61].

The SEM images of the fracture surfaces of OPC, NS10, SF10 and FA10 after 28 days of curing are given in Figure 8. The SEM images of OPC (Figure 8a), SF10 and FA10 (Figure 8c and 8d) display all hydrated cementious products including C–S–H. At the same time, deposits of small and large CH crystals are dispersed in the hardened cement mortars, which are often in OPC and are quite occasional in FA10 and SF10. The SEM image of NS10 (Figure 8b) differs from the SEM images of OPC, SF10 and FA10, where the texture of the hydration products is denser and more compact. Large crystals of CH are not observed all through the structure.

4. Conclusion

In the present study, the influence of high dosages of nano silica (NS) 5 wt% and 10 wt%, on the mechanical and structural properties of cement mortars at early (7th day) and standard (28th day) curing ages were studied and compared with the effects of equal amounts of the commercially used pozzolanic mineral additives silica fume (SF) and fly ash (FA). For dispersing NS, SF and FA particles in the mortar specimens properly, the colloidal mixture of each mineral additive in water was prepared by stirring at 15,000 rpm for 2 min prior to mixing with cement, fine aggregate, and the amount of hyperplasticizer was added.

The compressive strengths developed in the mortar specimens containing NS particles were found considerably higher than those of the corresponding specimens of SF and FA over and above the control at early and standard ages. Parallel to the increase in the amount of NS from 5 wt% to 10 wt%, the increases in compressive strength at both ages were observed. At standard age, the compressive strength of the mortar specimen with 10 wt% NS was 84% higher than that of the control, while the compressive strengths of the specimens with 10 wt% SF and 10 wt% FA were only 44% and 18% higher than that of the control. The increases in the flexural strengths of the mortars with 5 wt% and 10 wt% NS were also noticeable compared to the mortars with SF and FA on top of the control at standard age of curing.

The SEM images evidenced that NS was acting as nucleating agent for C–S–H gel formation from C_3S and C_2S. Nucleation appeared to occur along the entire surface of the NS particles, rather than at specific locations. FTIR and TG-DTG results supported the SEM observations. FTIR spectrum of the mortar with 10 wt% NS was the evidence for the highest degree of polymerization C_3S and C_2S phases with the formation of C–S–H phase compared to the mortars with SF and FA. TG-DTG results are in good agreement with FTIR results along with the highest compressive and flexural strengths observed in NS10. The extent of pozzolanic reactions was followed by monitoring the change in the amount of calcium hydroxide and of calcium carbonate, from the second and third steps of TG analyses, at early and standard ages for the samples containing 10 wt% NS, SF and FA. The amount of free CH and the total amount of CH and calcium carbonate of the mortar with 10 wt% NS were found the lowest among all the samples at both ages, suggesting the highest degree of bond formation between NS and calcium hydroxide.

Nano silica particles with the average size of 15 nm and the immense surface area of 640 $m^2.g^{-1}$ should have plenty of quantum sized pores and quantum sized tunnels, resulting in a pronounced surface reactivity. Accordingly, nano silica particles acted as nucleating agents and promoted hydration of C_3S and C_2S to produce prominent amount of C–S–H phase in comparison to silica fume and fly ash. Nano silica particles also possessed numerous active sites on their vast surfaces, such as broken Si–O– and Si– bonds, giving rise to very high pozzolanic reactivity and noticeable increase in the extent of bond formation with free calcium hydroxide.

Consequently, the use of nano silica can be assertively suggested to improve the structural characteristics and mechanical performance of cement mortars and concrete when compared to SF and FA. NS containing cement composites can be appropriate for many applications where early compressive strength is required, such as concrete roof tiles, masonry blocks, high strength mortars etc., and also for applications where improvement of flexural strength is essential especially for unreinforced cement composites

such as airport concrete pavements and roads for safely distributing concentrated loads over wide areas. Prior to the use of NS in concrete applications, further investigations must be performed for understanding the effect of NS on the permeability, water absorption, workability, long term durability and creeping of concrete, as well as the manufacturing, safety and handling issues of nano silica-supplemented cement mixtures, industrial scale-up of the laboratory processes and cost.

Moreover, determination of surface characteristics of pure nano silica particles and nano silica added cement pastes, such as surface area, surface roughness, pore volume, quantum sized pore distribution and macro quantum tunnel effects as well as surface free energy changes, can be carried out for clarifying the effect of nano-sized silica particles on the hydration mechanism of cement based composites, which will also need further study in the future.

Acknowledgements

This research was funded by Istanbul Kültür University (IKU). The authors wish to thank Gokcen Ukuser and Refik Arat for their assistances in FTIR and TG-DTA measurements, performed at IKU Materials Research Laboratory.

References

1. Bjornstrom J, Martinelli A, Matic A, Borjesson L and Panas I. Accelerating effects of colloidal nanosilica for beneficial calcium-silicate-hydrate formation in cement. *Chemical Physics Letters*. 2004; 392(1-3):242-248. http://dx.doi.org/10.1016/j.cplett.2004.05.071
2. Florence S and Konstantin S. Nanotechnology in concrete - A review. *Construction and Building Materials*. 2010; 24:2060-2071. http://dx.doi.org/10.1016/j.conbuildmat.2010.03.014
3. Shi C, Fernández Jiménez A and Palomo A. New cements for the 21st century: the pursuit of an alternative to Portland cement. *Cement and Concrete Research*. 2011; 41:750-763. http://dx.doi.org/10.1016/j.cemconres.2011.03.016
4. Pacheco-Torgal F, Miraldo S, Ding Y and Labrincha JA. Targeting HPC with the help of nanoparticles: An overview. *Construction and Building Materials*. 2013; 38:365-370. http://dx.doi.org/10.1016/j.conbuildmat.2012.08.013
5. Said AM, Zeidan MS, Bassuoni MT and Tian Y. Properties of concrete incorporating nano-silica. *Construction and Building Materials*. 2012; 36:838-844. http://dx.doi.org/10.1016/j.conbuildmat.2012.06.044
6. Zhang MH and Islam J. Use of nano-silica to reduce setting time and increase early strength of concretes with high volumes of fly ash or slag. *Construction and Building Materials*. 2012; 29:573-580. http://dx.doi.org/10.1016/j.conbuildmat.2011.11.013
7. Hou P, Kawashima S, Wang K, Corr DJ, Qian J and Shah SP. Effects of colloidal nanosilica on rheological and mechanical properties of fly ash-cement mortar. *Cement and Concrete Composites*. 2013; 35(1):12-22. http://dx.doi.org/10.1016/j.cemconcomp.2012.08.027
8. Jo BW, Kim CH, Tae G and Park JB. Characteristics of cement mortar with nano-SiO_2 particles. *Construction and Building Materials*. 2007; 21(6):1351-1355. http://dx.doi.org/10.1016/j.conbuildmat.2005.12.020
9. Mazloom M, Ramezanianpour AA and Brooks JJ.Effect of silica fume on mechanical properties of high-strength concrete. *Cement and Concrete Composites*. 2004; 26(4):347-357. http://dx.doi.org/10.1016/S0958-9465(03)00017-9
10. Garboczi EJ. Concrete nanoscience and nanotechnology, Definitions and applications. In: *Proceedings of the 3rd International Symposium on Nanotechnology in construction*; 2009; Prague. Prague; 2009. *p.* 81-88.
11. Gaitero JJ, Campillo I, Mondal P and Shah SP. Small changes can make a great difference. *Transportation Research Record*. 2010; 1(2141):1-5. http://dx.doi.org/10.3141/2141-01
12. Al-Amoudi OSB, Maslehuddin M and Abiola TO. Effect of type and dosage of silica fume on plastic shrinkage in concrete exposed to hot weather. *Construction and Building Materials*. 2004; 18:737-743. http://dx.doi.org/10.1016/j.conbuildmat.2004.04.031
13. Lee J, Mahendra S and Alvarez PJJ. Nanomaterials in the construction industry: a review of their applications and environmental health and safety considerations. *ACS Nano2010*. 2010; 4(7):3580-3590. http://dx.doi.org/10.1021/nn100866w
14. Mukhopadhyay AK. Next-generation nano-based concrete construction products. In: Gopalakrishnan K, Birgisson B, Taylor P, Attoh-Okine NO, editors. *A review. Nanotechnology in civil infrastructure*. Springer-Verlag Berlin Heidelberg; 2011. *p.* 207-223.
15. Li H, Xiao HG and Ou JP. A study on mechanical and pressure-sensitive properties of cement mortar with nanophase materials. *Cement and Concrete Research*. 2004; 34:435-438. http://dx.doi.org/10.1016/j.cemconres.2003.08.025
16. Qing Y, Zenan Z, Deyu K and Rongshen C. Influence of nano-SiO_2 addition on properties of hardened cement paste as compared with silica fume. *Construction and Building Materials*. 2007; 21(3):539-545. http://dx.doi.org/10.1016/j.conbuildmat.2005.09.001
17. Tao J. Preliminary study on the water permeability and microstructure of concrete incorporating nano-SiO_2. *Cement and Concrete Research*. 2005; 35:1943-1947. http://dx.doi.org/10.1016/j.cemconres.2005.07.004
18. Nazari A and Riahi S. The effects of SiO_2 nanoparticles on physical and mechanical properties of high strength compacting concrete. *Composites Part B*. 2011; 42:570-578. http://dx.doi.org/10.1016/j.compositesb.2010.09.025
19. Cwirzen A. Controlling physical properties of cementitious matrixes by nanomaterials. *Advanced Materials Research*. 2010; 123-125:639-642. http://dx.doi.org/10.4028/www.scientific.net/AMR.123-125.639
20. Givi AN, Rashid AS, Aziz FNA and Mohd Salleh MA. Particle size effect on the permeability properties of nano-SiO_2 blended Portland cement concrete. *Journal of Composite Materials*. 2011; 45(11):1173-1180. http://dx.doi.org/10.1177/0021998310378908
21. Hosseini P, Booshehrian A and Farshchi S. Influence of Nano-SiO_2 Addition on Microstructure and Mechanical Properties of CementMortars for Ferrocement. *Journal of the Transportation Research Board*. 2010; 2141:15-20. http://dx.doi.org/10.3141/2141-04

22. Pourjavadi A, Fakoorpoor SM, Hosseini P and Khaloo A. Interactions between superabsorbent polymers and cement-based composites incorporating colloidal silica nanoparticles. *Cement and Concrete Composites.* 2012; 37:196-204. http://dx.doi.org/10.1016/j.cemconcomp.2012.10.005
23. Li G. Properties of high-volume fly ash concrete incorporating nano-SiO_2. *Cement and Concrete Research*. 2004; 34(6):1043-1049. http://dx.doi.org/10.1016/j.cemconres.2003.11.013
24. Li H, Zhang M and Ou J. Abrasion resistance of concrete containing nano-particles for pavement. *Wear*. 2006; 260(11-12):1262-1266. http://dx.doi.org/10.1016/j.wear.2005.08.006
25. Shih JY, Chang TP and Hsiao TC. Effect of nanosilica on characterization of Portland cement composite. *Materials Science and Engineering*. 2006; 424(1-2):266-274. http://dx.doi.org/10.1016/j.msea.2006.03.010
26. Li H, Xiao HG, Yuan J and Ou J. Microstructure of cement mortar with nanoparticles. *Composites Part B*: Engineering. 2004;35(2):185-189. http://dx.doi.org/10.1016/S1359-8368(03)00052-0
27. Ab Rahman I and Padavettan V. Synthesis of silica nanoparticles by sol-gel: size-dependent properties, surface modification, and applications in silica-polymer nanocomposites—a review. *Journal of Nanomaterials*. 2012; Article ID 132424. http://dx.doi.org/10.1155/2012/132424
28. Lazaro A, Brouwers HJH, Quercia G and Geus JW. The properties of amorphous nano-silica synthesized by the dissolution of olivine. *Chemical Engineering Journal*. 2012; 211-212(15):112-121. http://dx.doi.org/10.1016/j.cej.2012.09.042
29. Senff L, João AL, Victor MF, Dachamir H and Wellington LR. Effect of nano-silica on rheology and fresh properties of cement pastes and mortars. *Construction and Building Materials*. 2009; 23(7):2487-2491. http://dx.doi.org/10.1016/j.conbuildmat.2009.02.005
30. Flores I, Sobolev K, Torres-Martinez LM, Cuellar EL, Valdez PL and Zarazua E. Performance of cement systems with Nano-SiO_2 particles produced by the sol-gel method. *Transportation Research Record*. 2010; 1(2141):10-14. http://dx.doi.org/10.3141/2141-03
31. Burgos-Montes O, Palacios M, Rivilla P and Puertas F. Compatibility between superplasticizer admixtures and cements with mineral additions. *Construction and Building Materials*. 2012; 31:300-309. http://dx.doi.org/10.1016/j.conbuildmat.2011.12.092
32. Berra M, Carassiti F, Mangialardi T, Paolini AE and Sebastiani M. Effects of nanosilica addition on workability and compressive strength of Portland cement pastes. *Construction and Building Materials*. 2012; 35:666-675. http://dx.doi.org/10.1016/j.conbuildmat.2012.04.132
33. Leemann A and Winnefeld F. The effect of viscosity modifying agents on mortar and concrete. *Cement and Concrete Composites*. 2007; 29(5):341-349. http://dx.doi.org/10.1016/j.cemconcomp.2007.01.004
34. Qing Y, Zenan Z, Li S and Rongshen C. A comparative study on the pozzolanic activity between nano-SiO_2 and silica fume. *Journal of Wuhan University of Technology Materials Science Edition*. 2008; 21(3):153-157. http://dx.doi.org/10.1007/BF02840907
35. Quercia G, Lazaro A, Geus JW and Brouwers HJH. Characterization of morphology and texture of several amorphous nano-silica particles used in concrete. *Cement and Concrete Composites*. 2013; 44:77-92. http://dx.doi.org/10.1016/j.cemconcomp.2013.05.006
36. Nanoamor-Europe. Available from: <http://www.nanoamor-europe.com/nanomaterials/nanoparticles/single-metal-oxides/sio2-nanopowders/>.
37. European Standards. *CSN EN 934-2*: Admixtures for concrete, mortar and grout - Part 2, Concrete admixtures - Definitions, requirements, conformity, marking and labeling. European Standards. Available from: <http://www.en-standard.eu/>.
38. European Commission for Standardization. *CEN EN 1015-3*: Methods of test for mortar for masonry. Determination of consistence of fresh mortar (by flow table). CEN; 1999. *p.* 1-10.
39. American Society for Testing and Materials - ASTM. *C39 / C39M-12*: Standard Test Method for Compressive Strength of Cylindrical Concrete Specimens. West Conshohocken: ASTM International; 2012. http://dx.doi.org/10.1520/C0039_C0039M-12
40. American Society for Testing and Materials - ASTM. *C348-08*: Standard Test Method for Flexural Strength of Hydraulic-Cement Mortars. West Conshohocken: ASTM International; 2008. http://dx.doi.org/10.1520/C0348-08
41. Xu P, Kirkpatrick RJ, Poe B, McMillan PF and Cong X. Structure of calcium silicate hydrate (C-S-H):near-, mid-, and far-infrared spectroscopy. *Journal of the American Ceramic Society*. 1999; 82(3):742-748.
42. Varas MJ, Alvarez de Buergo M and Fort R. Natural cement as the precursor of Portland cement: Methodology for its identification. *Cement and Concrete Research*. 2005; 35:2055-2065. http://dx.doi.org/10.1016/j.cemconres.2004.10.045
43. Ylmén R, Jäglid U, Steenari BM and Itai P. Early hydration and setting of Portland cement monitored by IR, SEM and Vicat techniques. *Cement and Concrete Research*. 2009; 39:433-439. http://dx.doi.org/10.1016/j.cemconres.2009.01.017
44. Kontoleontos F, Tsakiridis PE, Marinos A, Kaloidas V and Katsioti M. Influence of colloidal nanosilica on ultrafine cement hydration: Physicochemical and microstructural characterization. *Construction and Building Materials*. 2012; 35:347-360. http://dx.doi.org/10.1016/j.conbuildmat.2012.04.022
45. Yılmaz B and Olgun A. Studies on cement and mortar containing low-calcium fly ash, limestone, and dolomitic limestone. *Cement and Concrete Composites*. 2008; 30:194-201. http://dx.doi.org/10.1016/j.cemconcomp.2007.07.002
46. Chang C-F and Chen J-W. The experimental investigation of concrete carbonation depth. *Cement and Concrete Research*. 2006; 36:1760-1767 http://dx.doi.org/10.1016/j.cemconres.2004.07.025
47. Fernández-Carrasco L and Vázquez E. Reactions of fly ash with calcium aluminate cement and calcium sulphate. *Fuel*. 2009; 88:1533-1538. http://dx.doi.org/10.1016/j.fuel.2009.02.018
48. Parande AK, Ramesh Babu B, Pandi K, Karthikeyan MS and Palaniswamy N. Environmental effects on concrete using Ordinary and Pozzolana Portland cement. *Construction and Building Materials*. 2011; 25:288-297. http://dx.doi.org/10.1016/j.conbuildmat.2010.06.027
49. Esteves LP. On the hydration of water-entrained cement-silica systems, combined SEM, XRD and thermal analysis in cement pastes. *Thermochimica Acta*. 2011; 518:27-35. http://dx.doi.org/10.1016/j.tca.2011.02.003
50. Frias M and Cabrera J. Influence of MK on the reaction kinetics in MK/lime and MK-blended cement systems at 20°C. *Cement and Concrete Research*. 2001; 31:519-27. http://dx.doi.org/10.1016/S0008-8846(00)00465-8

51. Wongkeo W and Chaipanich A. Compressive strength, microstructure and thermal analysis of autoclaved and air cured structural lightweight concrete made with coal bottom ash and silica fume. *Materials Science and Engineering*. 2010; 527:3676-3684. http://dx.doi.org/10.1016/j.msea.2010.01.089

52. Ashraf M, Naeem Khan A, Ali Q, Mirza J, Goyal A and Anwar AM. Physico-chemical, morphological and thermal analysis for the combined pozzolanic activities of minerals additives. *Construction and Building Materials*. 2009; 23:2207-2213. http://dx.doi.org/10.1016/j.conbuildmat.2008.12.008

53. Aly M, Hashmi MSJ, Olabi AG, Messeiry M, Abadir EF and Hussain AI. Effect of colloidal nano-silica on the mechanical and physical behavior of waste-glass cement mortar. *Materials Design*. 2012; 33:127-135. http://dx.doi.org/10.1016/j.matdes.2011.07.008

54. Mleza Y and Hajjaji M. Microstructural characterisation and physical properties of cured thermally activated clay-lime blends. *Construction and Building Materials*. 2012; 26:226-232.

55. Tobón JI, Payá JJ, Borrachero MV and Restrepo OJ. Mineralogical evolution of Portland cement blended with silica nanoparticles and its effect on mechanical strength. *Construction and Building Materials*. 2012; 36:736-742. http://dx.doi.org/10.1016/j.conbuildmat.2012.06.043

56. Askarinejad A, Pourkhorshidi AR and Parhizkar T. Evaluation the pozzolanic reactivity of sonochemically fabricated nano natural pozzolan. *Ultrason Sonochem*. 2012; 19:119-124. http://dx.doi.org/10.1016/j.ultsonch.2011.05.005

57. Feldman RF and Ramachandran VS. Differentiation of interlayer and adsorbed water in hydrated Portland cement by thermal analysis. *Cement and Concrete Research*. 1971; 1:607-620. http://dx.doi.org/10.1016/0008-8846(71)90016-0

58. Stefanidou M and Papayianni I. Influence of nano-SiO_2 on the Portland cement pastes. *Composites:* Part B. 2012; 43(6):2706-2710. http://dx.doi.org/10.1016/j.compositesb.2011.12.015

59. Lindgreen H, Geiker M, Krøyer H, Springer N and Skibsted J. Microstructure engineering of Portland cement pastes and mortars through addition of ultrafine layer silicates. *Cement and Concrete Composites*. 2008; 30(8):686-699. http://dx.doi.org/10.1016/j.cemconcomp.2008.05.003

60. Min-Hong Z, Jahidul I and Sulapha P. Use of nano-silica to increase early strength and reduce setting time of concretes with high volumes of slag. *Cement and Concrete Composites*. 2012; 34(5):650-662. http://dx.doi.org/10.1016/j.cemconcomp.2012.02.005

61. Monteiro PJM, Kirchheim AP, Chae S, Fischer P, MacDowell AA, Schaible E et al. Characterizing the nano and micro structure of concrete to improve its durability. *Cement and Concrete Composites*. 2009; 318:577-584. http://dx.doi.org/10.1016/j.cemconcomp.2008.12.007